Environmental Science & Technology

pubs.acs.org/est

Article

Climate Effects on Subsoil Carbon Loss Mediated by Soil Chemistry

Angela R. Possinger, Tyler L. Weiglein, Maggie M. Bowman, Adrian C. Gallo, Jeff A. Hatten, Katherine A. Heckman, Lauren M. Matosziuk, Lucas E. Nave, Michael D. SanClements, Christopher W. Swanston, and Brian D. Strahm*

Cite This: *Environ. Sci. Technol.* 2021, 55, 16224−16235

Read Online

ACCESS | Metrics & More | Article Recommendations | Supporting Information

ABSTRACT: Subsoils store at least 50% of soil organic carbon (SOC) globally, but climate change may accelerate subsoil SOC (SOC_{sub}) decomposition and amplify SOC-climate feedbacks. The climate sensitivity of SOC_{sub} decomposition varies across systems, but we lack the mechanistic links needed to predict system-specific SOC_{sub} vulnerability as a function of measurable properties at larger scales. Here, we show that soil chemical properties exert significant control over SOC_{sub} decomposition under elevated temperature and moisture in subsoils collected across terrestrial National Ecological Observatory Network sites. Compared to a suite of soil and site-level variables, a divalent base cation-to-reactive metal gradient, linked to dominant mechanisms of SOC_{sub} mineral protection, was the best predictor of the climate sensitivity of SOC decomposition. The response was "U"-shaped, showing higher sensitivity to temperature and moisture when either extractable base cations or reactive metals were highest. However, SOC_{sub} in base cation-dominated subsoils was more sensitive to moisture than temperature, with the opposite relationship demonstrated in reactive metal-dominated subsoils. These observations highlight the importance of system-specific mechanisms of mineral stabilization in the prediction of SOC_{sub} vulnerability to climate drivers. Our observations also form the basis for a spatially explicit, scalable, and mechanistically grounded tool for improved prediction of SOC_{sub} response to climate change.

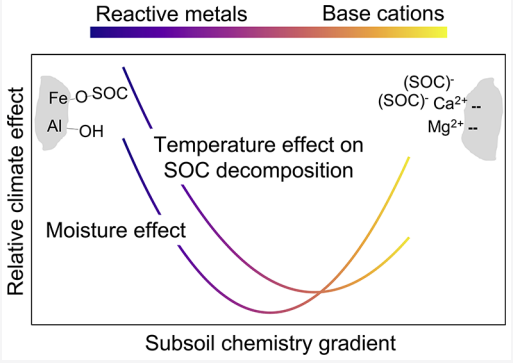

KEYWORDS: *subsoil carbon, organo-mineral, climate sensitivity, base cation, reactive metal*

INTRODUCTION

Globally, soils provide the largest terrestrial carbon (C) reservoir, and 50−70% of the soil organic carbon (SOC) stock is stored in subsoils (deeper than ∼20−30 cm).[1−3] On a yearly timescale, the difference between SOC acting as a global net source or sink of CO_2 is small (<5 Gt C yr^{-1}) in comparison to the SOC stock (1500−2400 Gt C).[3,4] The climate sensitivity of SOC decomposition is a critical driver of widely divergent long-term SOC stock predictions, which range from soil as a net sink to a significant net source of carbon dioxide (CO_2) under climate change.[5] Even relatively minor increases in SOC mineralization rates resulting from changing climate drivers could have an outsized influence on the biosphere-atmosphere C flux.[6,7]

Though subsoil SOC (SOC_{sub}) is generally older and more protected from microbial access relative to topsoil SOC,[8,9] subsoil respiration can account for up to 25% of the total soil CO_2 flux under experimental warming,[10] and emerging evidence suggests that SOC_{sub} mineralization rates can be equally or more sensitive to environmental change.[10,11] However, quantifying and predicting temperature and moisture effects on SOC_{sub} mineralization is complicated by divergence in controls on SOC cycling between sub- and surface soils[12] and is further compounded by variability in SOC sources and subsoil properties at different spatial locations and scales.[13−15] In this work, we assessed whether accounting for soil chemical properties linked with expected dominant mechanism of mineral-SOC association[16] could improve representation of divergent controls on SOC_{sub} climate sensitivity.

A range of physicochemical mechanisms that vary as a function of soil and ecosystem properties contribute to mineral SOC stabilization.[17−21] Evidence from experimental, theoretical, and direct observation approaches supports a link between exchangeable divalent base cations and cation bridging, organo-organic cross-linkages, and/or minor amounts of inner-sphere complexation; in contrast, a larger contribution of inner-sphere interactions has been associated with abundance of semi- or non-crystalline metals (e.g., see refs 18−22 and references within). A shift in these dominant

Received: July 22, 2021
Revised: November 4, 2021
Accepted: November 8, 2021
Published: November 23, 2021

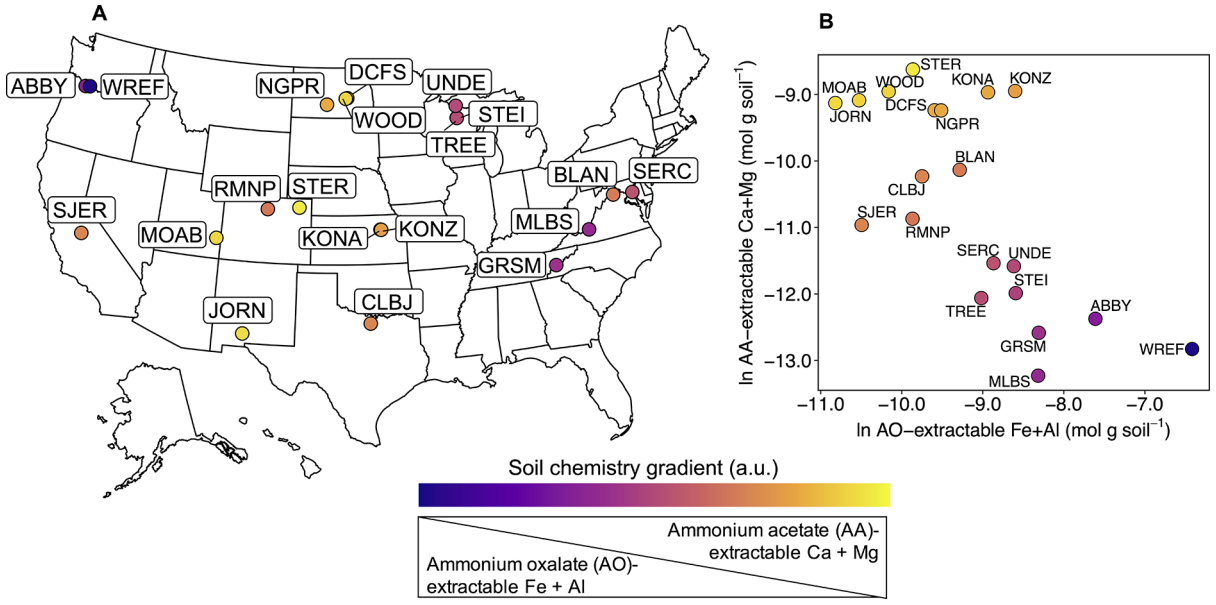

Figure 1. Continental-scale soil chemistry gradient used to test the effects of elevated temperature and moisture on subsoil SOC (SOC_{sub}) decomposition. (A) Soils were collected within the eddy covariance (flux) tower footprint at conterminous US NEON sites. Full site names and further site information are listed in Table 1. (B) Distribution of sites along the soil chemistry gradient from higher abundance of ammonium (NH_4^+) oxalate (AO)-extractable iron (Fe) plus aluminum (Al) (here called "reactive metals") to higher abundance of NH_4^+ acetate (AA)-extractable calcium (Ca) plus magnesium (Mg) ("base cations") (both ln-transformed), based on upper B-horizon soil measurements. Points are colored by the first principal component axis, a linear combination of the *X* and *Y* axes (a.u. indicates arbitrary units).

mechanisms of interaction has implications for the reversal of SOC protection via mineral associations (i.e., SOC destabilization).[18,22−26] In lieu of a direct means to represent microscale desorption processes at biogeochemical model-relevant scales, soil chemical and climate proxies for the dominant type of mineral-SOC association (e.g., extractable metals, soil pH, and climate variables) have been employed to statistically model SOC cycling metrics, including SOC contents and the proportion of mineral-associated SOC.[16,27]

While up to ∼70% of SOC may be protected by reactive mineral association in some systems,[27] mineral-SOC associations are reversible, and transformations of mineral-protected SOC can be driven by changes to the soil environment, including increased temperature or changes in moisture availability.[28,29] Moreover, SOC resistance to decomposition is also conferred by a variety of different mechanisms in addition to mineral association, including spatial discontinuity between microbes and organic substrates, and environmental constraints on microbial physiology.[29,30] The relative importance of these mechanisms driving SOC stabilization varies spatially,[30] and as such, SOC is not expected to be equally sensitive to changes in temperature and moisture across space.[31−33] Therefore, application of fixed temperature and moisture corrections regardless of soil type and dominant mode of SOC protection may bias modeled projections of SOC_{sub} loss under climate change,[34,35] especially when net SOC_{sub} loss due to high climate sensitivity of decomposition may offset accrual.[5] Furthermore, temperature and moisture responses associated with different mechanisms of stabilization are unknown at scales relevant for Earth system models that couple climate and terrestrial biogeochemistry. In particular, climate sensitivity linked to variation in the dominant mechanism of mineral-facilitated SOC_{sub} stabilization has not been considered in the context of covarying drivers of SOC_{sub} climate sensitivity at model-relevant scales, including variation in climate and SOC_{sub} composition.

Here, we assessed how the expected mechanism of mineral interaction modifies SOC_{sub} climate sensitivity using a continental-scale subsoil chemistry gradient from high extractable base cations (from here called "base cations") to high extractable non- and semi-crystalline metals ("reactive metals"). This well-described dichotomy in soil chemistry is tied to often co-varying gradients in moisture availability, leaching potential, parent materials, soil pH, and major vegetation groups (i.e., grasslands vs forests).[14−16] Like soil pH and aridity indices,[16,27] this soil chemistry gradient may serve as a proxy for representation of divergent controls on SOC cycling across ecosystems. However, we posit that the abundance of reactive elements that contribute to mineral surface chemistry may provide a stronger conceptual link to climate-driven destabilization of mineral surface-associated SOC_{sub}. Consequently, we hypothesized that this gradient would serve as a quantifiable and spatially explicit means of improving our predictions of SOC_{sub} mineralization sensitivity to increased temperature and moisture when mineral protection is expected to be a dominant SOC_{sub}-stabilizing process. To investigate the sensitivity of SOC_{sub} decomposition to climate drivers, we combined cumulative specific respiration (CSR) temperature and moisture response measurements derived from laboratory incubations with a suite of soil and site-level variables derived from National Ecological Observatory Network (NEON; neonscience.org) sites distributed across the conterminous US.

MATERIALS AND METHODS

Study Sites. The climate sensitivity of SOC_{sub} mineralization was determined for subsoils from 20 NEON sites in the conterminous US, selected based on expected influence of soil chemistry on SOC_{sub} temperature and moisture response

https://doi.org/10.1021/acs.est.1c04909
Environ. Sci. Technol. 2021, 55, 16224−16235

(Figure 1, Table 1, Supporting Information 1.1, Figures S1 and S2, Table S1). Land use at these sites includes unmanaged wildland, managed grasslands, regenerating agriculture, and agriculture (Table S2). Lime has not been applied at any of the studied NEON sites since site installation. Site-level climate variables are described in refs 14 and 15. Briefly, mean annual temperature (MAT), mean annual precipitation (MAP), MAP−Hargreaves reference evaporation (E_{ref}) (i.e., "aridity index"), and relative humidity (RH) were obtained from the ClimateNA_MAP database[36] and shown as averages over the period 1961−1990 (Table S3). Site-level net primary production (NPP) (kg C m^{-2} yr^{-1}) was determined using MODIS data (Table S3).[37,38] Site mean summer temperature (MST) was obtained from PRISM[39] (Table S3). Definitions and derivations for climate variables are summarized in Table S4.

Table 1. Site Names, Locations, and Dominant Soil Orders for NEON Sites Used to Assess Soil Chemistry Effects on Subsoil SOC Climate Sensitivity[a]

site ID	site name	latitude (dec. °N)	longitude (dec. °W)	soil order
ABBY	Abby Road	45.762	−122.330	Inceptisol
BLAN	Blandy Experimental Farm	39.060	−78.072	Alfisol
CLBJ	LBJ/Caddo	33.401	−97.570	Alfisol
DCFS	Dakota-Coteau	47.162	−99.107	Mollisol
GRSM	Great Smoky Mountain National Park	35.689	−83.502	Inceptisol
JORN	Jornada	32.591	−106.843	Aridisol
KONA	Konza Agriculture	39.110	−96.613	Mollisol
KONZ	Konza Core	39.101	−96.563	Mollisol
MLBS	Mountain Lake	37.378	−80.525	Entisol
MOAB	Moab	38.248	−109.388	Aridisol
NGPR	Northern Great Plains Research Laboratory	46.770	−100.915	Mollisol
RMNP	Rocky Mountain National Park	40.276	−105.546	Inceptisol
SERC	Smithsonian Environmental Research Center	38.890	−76.560	Ultisol
SJER	San Joaquin	37.109	−119.732	Alfisol
STEI	Steigerwalt	45.509	−89.586	Spodosol
STER	Sterling	40.462	−103.029	Mollisol
TREE	Treehaven	45.494	−89.586	Spodosol
UNDE	UNDERC	46.234	−89.537	Spodosol
WOOD	Woodworth	47.128	−99.241	Mollisol
WREF	Wind River	45.820	−121.952	Andisol

[a]UNDERC = University of Notre Dame Environmental Research Center; LBJ = Lyndon B. Johnson National Grassland.

Soil Sampling and Processing. This work utilized an archive of deep (up to approximately 2 m, bedrock, or refusal) soil cores collected within the micrometeorological flux tower footprint at terrestrial NEON sites, as described in refs 14 and 15 (4.5 cm-dia. Giddings probe) (Giddings Machine Company, Windsor, CO). At Wind River, five 3.45 cm diameter soil cores were collected using a handheld AMS corer (AMS Inc., American Falls, ID, USA) to a depth of 0.5 m. Soil cores were collected during NEON soil sensor array installation over the period of 2015−2018. Soil cores were stored cool (in coolers with ice packs) for transport, and processed as described in ref 15. Genetic horizons at similar depths and with similar diagnostic pedogenic features were pooled to generate one composite bulk soil sample per horizon per site. These composite samples were air-dried and sieved to 2 mm mesh to form a sample archive for 40 NEON sites, described in ref 15. A subset of archived soils were used for climate response studies (see Supporting Information 1.1 for further details on site selection). Briefly, a subset of archived soils (n = 29) were used for incubation experiments, selected to represent the range of soil properties across the NEON network (Figure S1). From incubated sites, a subset of soils with expected high contribution of mineral control on SOC_{sub} stabilization (n = 20) were used to assess the role of the mineral interaction mechanism in climate sensitivity, based on the absence of extreme climate controls (e.g., MAT < ∼0 °C) or low proportion of SOC in the dense fraction (DF) (i.e., mineral-associated SOC) (Table S1). All subsequent analyses are described for one bulk, composited subsoil (upper B-horizon) sample from each of the 20 sites with expected mineral influence on SOC turnover. The upper B-horizon midpoint depth ranged from approximately 18−58 cm, with a mean of approximately 38 cm (±12 s.d.) (Table S3).

Soil Characterization. *Extractable Metals and Basic Soil Properties.* Basic soil characterization data and analysis methods are published in refs 14 and 15 (Table S3). Briefly, extractable elements (including Ca and Mg) (i.e., base cations) were determined by ammonium (NH_4^+) acetate (AA) extraction following USDA NRCS protocols.[40] Reactive Fe and Al were determined by acid NH_4^+ oxalate (AO) extraction following USDA NRCS protocols.[40] Here, we consider the term "reactive metals" to be inclusive of AO-extractable non- and semi-crystalline oxide, aluminosilicate, and organically complexed Fe and Al, following refs 41−43.

Soil texture was determined by the laser diffraction method with an adjusted <0.6 μm particle diameter cutoff for clay.[44,45] Three cycles of water-bath sonication were used to disrupt aggregates between hydrogen peroxide treatments. Soil pH was determined in water at a 1:2 soil/water ratio after 10 min of equilibration, following ref 46. Total C and N were determined using an elemental analyzer-isotope ratio mass spectrometer (IsoPrime 100 EA-IRMS) (IsoPrime Ltd, Cheadle, UK). Samples with a "k" (carbonates) horizon suffix [determined by 10% hydrochloric acid (HCl) effervescence] were acidified by fumigation with HCl prior to EA-IRMS analysis, and the inorganic carbon (IC) content was determined by difference.[47]

SOC Age and Composition. Bulk radiocarbon depletion ($\Delta^{14}C$, per mil) was determined by accelerator mass spectrometry according to refs 48−50 and published in detail in ref 14 (Figure S3). For reference, further details of radiocarbon analysis are included in Supporting Information 1.2. The pyrogenic (i.e., fire-derived, condensed polyaromatic) C content was quantified using benzene polycarboxylic acid (BPCA) quantification (following ref 51) and is published in ref 14 (Figure S3). Further details of BPCA analysis are included in Supporting Information 1.3.

Density distribution of SOC into the free light fraction (FLF) and DF was determined following refs 52−55 and is also described in ref 56. Sodium polytungstate (SPT) solution was adjusted to a density of 1.65 g cm^{-3} and sonication applied at 750 J g $soil^{-1}$ (20 g of soil in 50 mL SPT, sonicated for 5 min at a rate of 50 J s^{-1}, corresponding to 1500 J total, or 30 J mL^{-1}). Total organic C of density fractions was determined using an IsoPrime 100 EA-IRMS instrument (IsoPrime Ltd, Cheadle, UK). Water-extractable OC (WEOC) (also described in ref 56) was determined by extraction at a 1:30 soil water

https://doi.org/10.1021/acs.est.1c04909
Environ. Sci. Technol. 2021, 55, 16224−16235

ratio, with 2 h shaking at 20 °C followed by centrifugation (8 min at 3824 rcf) and filtration with combusted glass fibers (Whatman GF/F, 0.7 μm pore size). Total organic C concentrations in extracts were determined using a Shimadzu TOC-V (Shimadzu Scientific Instruments, Columbia, MD, USA) analyzer with non-dispersive infrared (NDIR) detection. Samples were acidified within the TOC instrument and sparged prior to oxidation and combustion.

Soil Chemistry Axis Computation. For the 20 sites falling on the gradient from higher Ca and Mg to higher Fe and Al, the first principal component axis of the two mineralogical axes was computed using the "stats" package ("prcomp" function, centered and scaled) in R (v. 3.5.3)[57] in RStudio (v. 1.1.423),[58] using natural log-transformed AO-extractable Fe + Al (mol g dry soil^{-1}) and natural log-transformed AA-extractable Ca + Mg (mol g dry soil^{-1}). The first principal component axis is from here described as the "soil chemistry axis." In addition, we split the sites into subsystems, where sites below zero (n = 8 sites) or above zero (n = 12 sites) on the soil chemistry gradient were defined as reactive metal or base cation subsystems, respectively. The division into subsystems also coincided with a natural break-point in abundance of AA- and AO-extractable elements along the computed soil chemistry axis (Figure 1).

Temperature and Moisture Sensitivity of Mineralization. The response of CSR (cumulative respiration normalized to the initial SOC content) to warming and moisture was determined using a fully factorial temperature- and moisture-controlled laboratory incubation experiment. Incubations were conducted over the period 2016−2020. Reference 56 includes the incubation methodology for 365 d incubations of A and upper B-horizons conducted at MST and field capacity (−33 kPa). In this study, we used bulk (<2 mm) upper B horizon soils (drawn from a five-core composite sample, n = 1 for each temperature-by-moisture-by-site treatment combination) incubated for 91 d at temperature levels corresponding to the site MST and at MST +5 °C (Table S5) and variable moisture levels (−400, −150, and −33 kPa). These temperature levels were selected to elicit a strong potential warming response within the timeframe of the incubation. For incubation temperature bins, MST was used to represent temperatures experienced at the site during warmer seasons, when SOC mineralization is expected to be highest. At 32.5 °C, the highest incubation temperature is below the threshold expected for inhibitory effects of high temperature on soil respiration.[59] Incubation temperature was within an average 0.4 °C (±1.3 °C) of site MST or MST +5 °C for each temperature bin and maintained at ±0.5 °C in 566 L incubator units (VWR model 10753-894; VWR International, LLC, Radnor, PA, USA). For each site, 10−20 g of upper B horizon soil samples (air-dry, <2 mm) was incubated in approximately 120 mL polypropylene specimen cups within ∼1 or 0.5 L glass Mason jars fitted with air-tight butyl rubber septa.

Water potential was adjusted to and maintained throughout the incubation experiment to −400, −150, and −33 kPa (within 6 ± 7 s.d. % variation) with deionized (DI) water weight adjustments estimated using a soil texture-based pedotransfer function.[60] These water potential levels (−33, −150, and −400 kPa) coincide with optimal conditions for bacterial growth and movement, limited bacterial movement, and limited bacterial growth, respectively.[61] For each site, soil texture was estimated using NEON site Megapit soil texture measurements[62] or the USDA NRCS Web Soil Survey.[63] Soils were packed within specimen cups to an approximate bulk density of 1.2 g cm^{-3} (approximately 50% porosity). This value was selected based on the mean of available NEON site Megapit bulk density measurements at the time of incubation initiation. A consistent bulk density was used as a means to reduce sources of error in adjustments of the water content based on pedotransfer functions. To prevent drying, less than 10 mL of DI water was maintained in the base of each jar.

Incubation headspace gas sampling is described in ref 56. Briefly, the headspace gas carbon dioxide (CO_2) concentration was measured at time intervals determined by the previous cycle respiration rate, which was estimated by measuring headspace CO_2 on a LI-COR LI-6250 unit (LI-COR Biosciences, Lincoln, NE, USA) at the time of sampling (Figure S4). Evolved CO_2 was determined relative to measured initial ambient CO_2 (∼370−400 ppm CO_2) (Figure S4). This sampling regime resulted in headspace CO_2 concentrations within the range of instrument calibration (∼370 to 10,000 ppm CO_2). Headspace samples were collected in gas-tight glass gas chromatography (GC) vials. After sampling, jar lids were opened to vent each jar to ambient air. The CO_2 concentration of headspace samples was determined using a GC-2010 instrument (Shimadzu Scientific Instruments, Columbia, MD, USA) equipped with a methanizer and flame ionization detector. The CO_2 concentration was corrected for abiotic CO_2 evolution from carbonate dissolution in samples with the substantial carbonate content (indicated by the presence or absence of HCl effervescence and designated by a "k" horizon suffix) using solid and gas phase $\delta^{13}C$ measurements.[64] Solid-phase and gas-phase $\delta^{13}C$ measurements were made using an IsoPrime 100 EA-IRMS (Isoprime Ltd, Cheadle, UK) and a Thermo Scientific Delta V IRMS (Thermo Fisher Scientific, Waltham, MA), respectively. A three end-member mixing model was used to correct for inorganic CO_2 production, using measured $\delta^{13}C$ of CO_2 in ambient air, CO_2 produced during incubation, and solid-phase soil organic and inorganic C.

Cumulative total CO_2−C mineralized (0−91 days) (total respiration flux) was determined by summation of CO_2−C (mg CO_2−C g soil^{-1}) at each measurement timepoint. Cumulative CO_2−C was normalized by the initial SOC content to determine CSR (mg CO_2−C g initial SOC^{-1}). To emphasize contrasts between climate effects, temperature effects were assessed by calculation of the ln-transformed ratio of CSR at MST +5 °C to CSR at MST. To represent the highest potential moisture response (Figure S5) (see "ANOVA" methods below), moisture effects were determined using the ln-transformed ratio of CSR at −33 to −400 kPa.

Statistical Analyses. All statistical analyses were conducted using R (v. 3.5.3)[57] in RStudio (v. 1.1.423)[58] using the base R "stats" package[57] unless noted otherwise. Detailed descriptions of statistical approaches, including estimation of model root mean squared error (RMSE) and comparison of ln-transformed versus non-transformed models, are included in Supporting Information 1.4.

Subsystem Comparisons. To compare SOC properties between subsystems [i.e., CSR under ambient conditions ($CSR_{ambient}$), bulk soil radiocarbon content, C/N ratio, pyrogenic C content, and proportion of C in the FLF and DF], we used a two-sided Wilcoxon Rank Sum test with continuity correction for approximated p-values (Figure S3, Table S6).

https://doi.org/10.1021/acs.est.1c04909
Environ. Sci. Technol. 2021, 55, 16224−16235

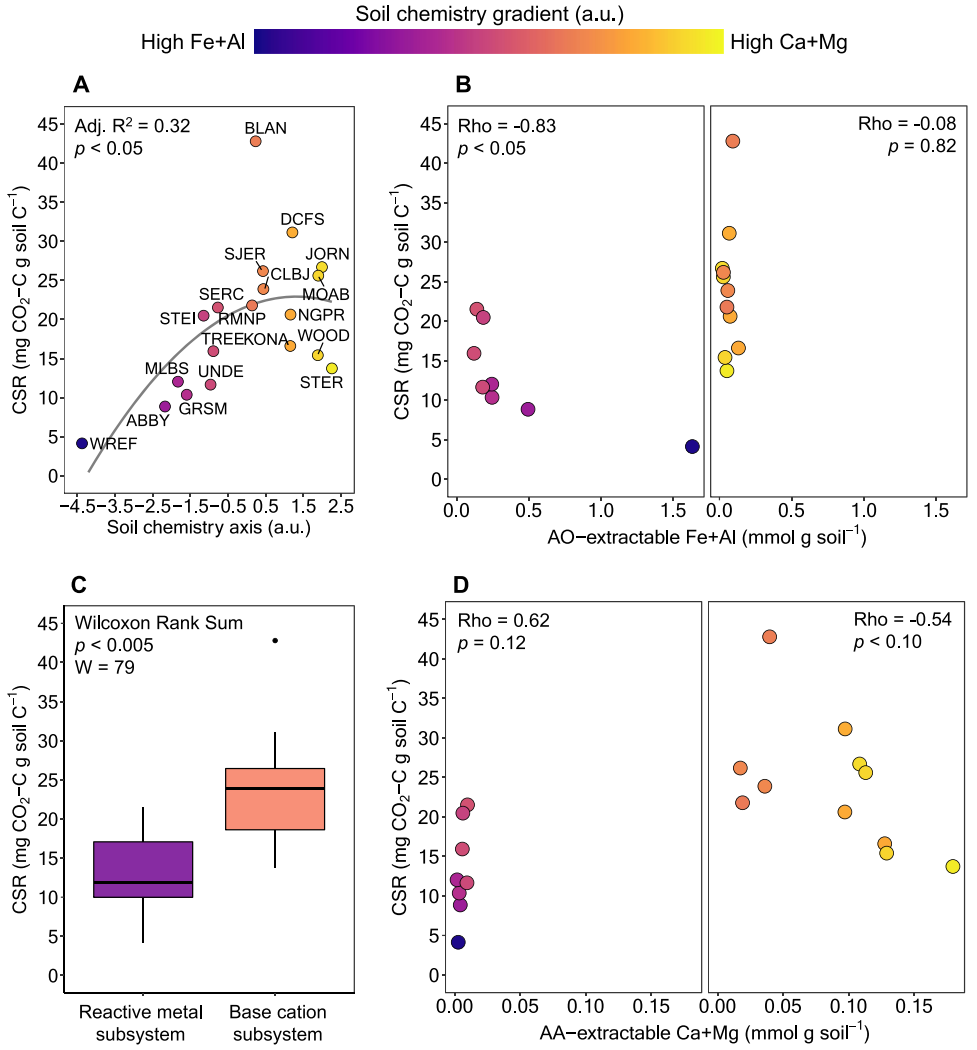

Figure 2. Subsoil SOC destabilization as a function of soil chemistry. (A,C) Subsoil SOC (SOC_{sub}) CSR under ambient temperature (site MST) and −150 kPa moisture ($CSR_{ambient}$) across a subsoil soil chemistry gradient (n = 19 sites) (a.u. indicates arbitrary units; gradient defined in Figure 1). In (C), points are grouped by soil chemistry axis values <0 (reactive metal subsystem) and >0 (base cation subsystem). Points show values for individual sites. Upper edges of boxes show first and third quartiles (25th and 75th percentiles), and lower and upper whiskers show the smallest and largest value no further than 1.5*interquartile range (IQR) of the box edges, while solid points indicate outliers beyond the 1.5*IQR. (B,D) Spearman correlations (Rho) between $CSR_{ambient}$ and either extractable reactive metals (B) or base cations (D). Full site names are listed in Table 1.

Temperature and Moisture Effects on CSR. Individual incubation jars with known jar seal failure or CSR more than ±2 standard deviation from site mean (all treatments, total n = 6 jars per site) were excluded from CSR ratio calculations.

ANOVA. Interactions between moisture and temperature treatments and differences in moisture response ratios (i.e., −33/−400, −33/−150, and −150/−400 kPa) were assessed by type II two-way or one-way ANOVA ("car" package[65]) (Figure S5, Table S7). Differences in the CSR ratio between soils with higher Ca and Mg or higher Fe and Al accounting for incubation temperature (MST or MST +5 °C) and moisture treatments (−400, −150, and −33 kPa) and interaction effects were determined with type II two-way ANOVA (Table S7). To reduce undue influence of outlier points, the ln-transformed CSR ratios were square-root transformed for ANOVA tests. Residuals versus fitted, normal Q−Q, scale-location, and residuals versus leverage plots were inspected to assess model assumptions.

Polynomial Regression. The relationship between temperature and moisture effects (at −150 kPa and MST, respectively) and the soil chemistry axis was assessed using second-order polynomial regression (Table S8). The relationship between $CSR_{ambient}$ and the soil chemistry axis was also assessed using a second-order polynomial fit (Table S8). The difference in fit between moisture and temperature treatments (for temperature and moisture effects, respectively) was assessed with a model type II ANOVA (Table S7). Additionally, relationships between the soil chemistry axis, correlated variables, and other soil properties commonly assumed to have a relationship with SOC accumulation were assessed by first- or second-order polynomial regression (Tables S9 and S10). In the absence of overall temperature by moisture interactions (Figure S5), all regression analyses were conducted using "ambient" conditions; that is, temperature effects were calculated at −150 kPa, and moisture effects at ambient temperature (MST), resulting in 19 independent sites due to individual jar exclusion described above. Second-

https://doi.org/10.1021/acs.est.1c04909
Environ. Sci. Technol. 2021, 55, 16224−16235

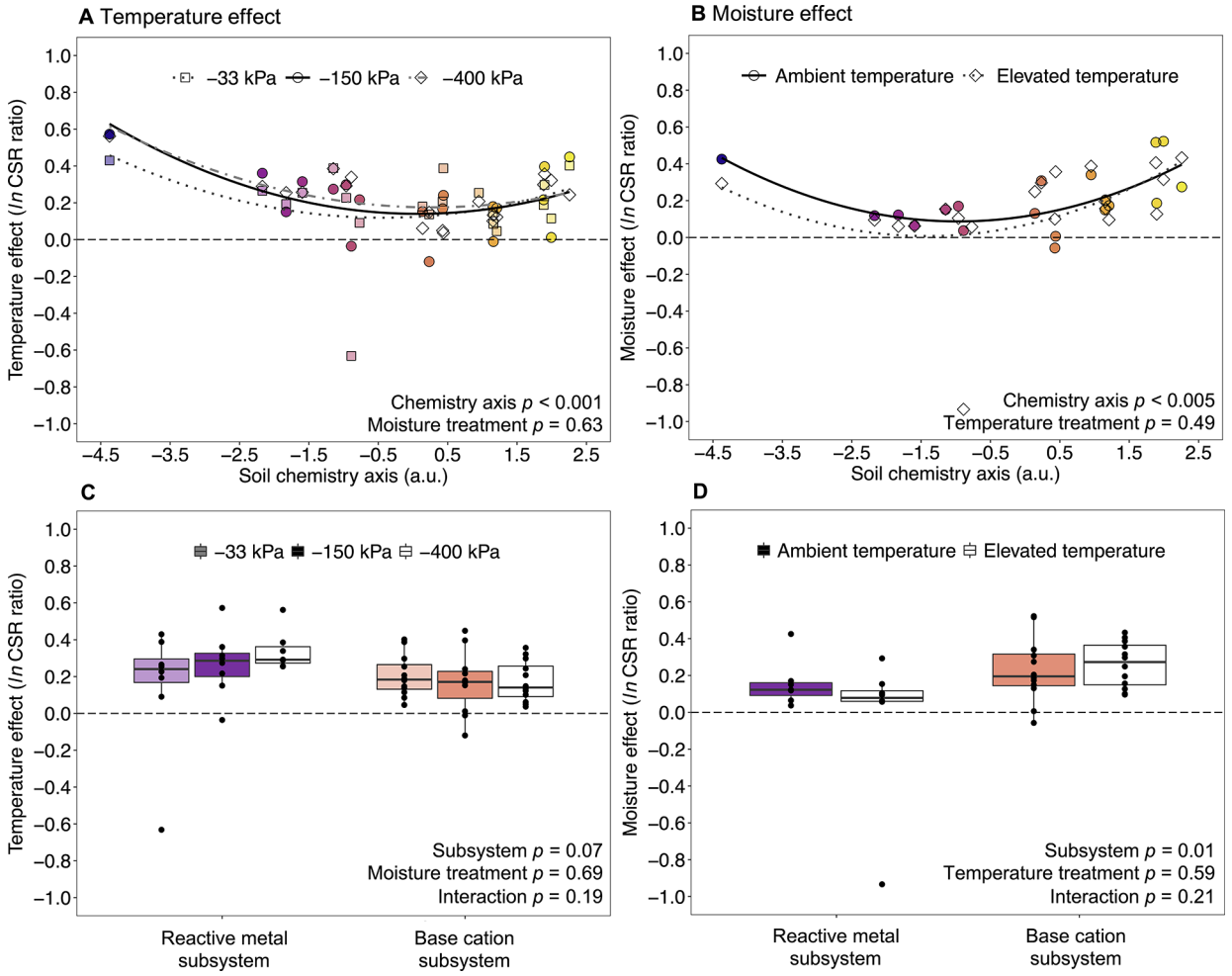

Figure 3. Climate effects of elevated temperature and moisture on subsoil SOC (SOC_{sub}) CSR across a subsoil soil chemistry gradient (a.u. indicates arbitrary units; gradient defined in Figure 1). (A) Temperature effect is shown as the ln-transformed ratio of CSR (mg CO_2−C g initial soil C^{-1}) between elevated (site MST, +5 °C) and ambient temperature (MST), at three experimental moisture levels: −400 kPa (n = 20), −150 kPa (n = 19), and −33 kPa (n = 20). (B) Moisture effect is shown as the ln-transformed ratio of CSR between the highest (−33 kPa) and lowest (−400 kPa) moisture treatments calculated at ambient temperature (n = 19) and elevated temperature (+5 °C) (n = 20). In (C,D), points show individual site-by-temperature-by-moisture observations. Lower and upper edges of boxes show first and third quartiles (25th and 75th percentiles), and lower and upper whiskers show the smallest and largest value no further than 1.5*IQR of the box edges, while solid points indicate outliers beyond the 1.5*IQR. For higher base cation soils, each boxplot shows 12 independent sites, except for the moisture effect at ambient temperature and temperature effect at −150 kPa (n = 11). For higher reactive metal soils, each boxplot shows eight independent sites, except for the temperature effect at −400 kPa (n = 7).

order polynomial fits were applied only when the adjusted R^2 improved (accounting for the addition of additional model terms) relative to a simple first-order linear fit. Distribution of model residuals was also used as an indicator of second-order relationships.

Spearman Rank Correlation. Spearman Rank tests with continuity correction for approximated coefficients were used to test correlations between $CSR_{ambient}$ and extractable element contents and $CSR_{ambient}$ and climate effects (Table S11).

Principal Component Analysis. Directionality and magnitude of relationships among the soil chemistry axis, temperature and moisture effects, site-level variables, and soil physicochemical properties were assessed by principal component analysis (PCA). All variables were ln-transformed prior to PCA to increase resolution of variable loadings. Principal components were computed as centered (each variable mean-subtracted) and scaled (each variable normalized by standard deviation).

RESULTS AND DISCUSSION

Mineral Controls on SOC_{sub} Persistence across a Soil Chemistry Gradient. Using a second-order polynomial, the continuous soil chemistry axis was a significant predictor of CSR under ambient conditions (i.e., −150 kPa moisture and MST) ($CSR_{ambient}$) (Figure 2A). Overall, $CSR_{ambient}$ was lower in the reactive metal subsystem (Figure 2C). In the reactive metal subsystem, lower SOC bioavailability (i.e., decreased $CSR_{ambient}$) was strongly correlated with increasing reactive metal content (Figure 2B), consistent with an increase in SOC protection by non- or semi-crystalline metals.[16,18] In contrast, when Fe and Al were low, $CSR_{ambient}$ was negatively correlated with increasing base cation content (Figure 2D). These relationships provide evidence for SOC_{sub} stabilization (in this case, via the metric of SOC_{sub} potential mineralization) correlated to abundance of extractable base cations or reactive metals.[16] In addition, higher base cation or reactive metal abundance had an effect on CSR only within the respective soil

https://doi.org/10.1021/acs.est.1c04909
Environ. Sci. Technol. 2021, 55, 16224−16235

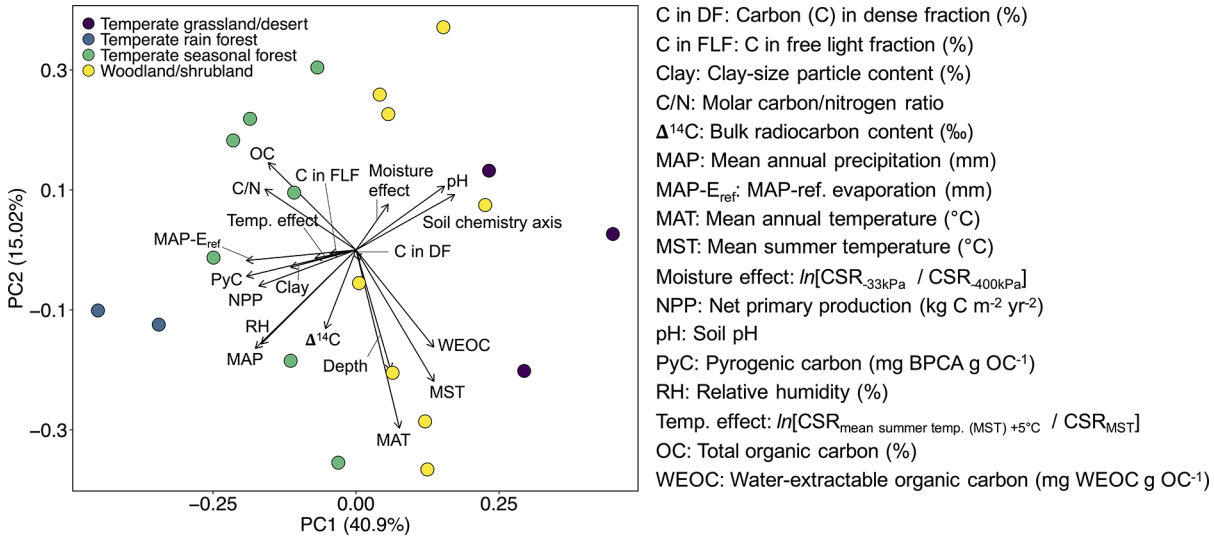

Figure 4. Principal component analysis of soil and site-level variables (n = 20 sites). Moisture and temperature effects are CSR ratios calculated at ambient temperature and −150 kPa moisture, respectively. Points show individual sites, with point fill defined by Whittaker biome. BPCA = benzene polycarboxylic acid.

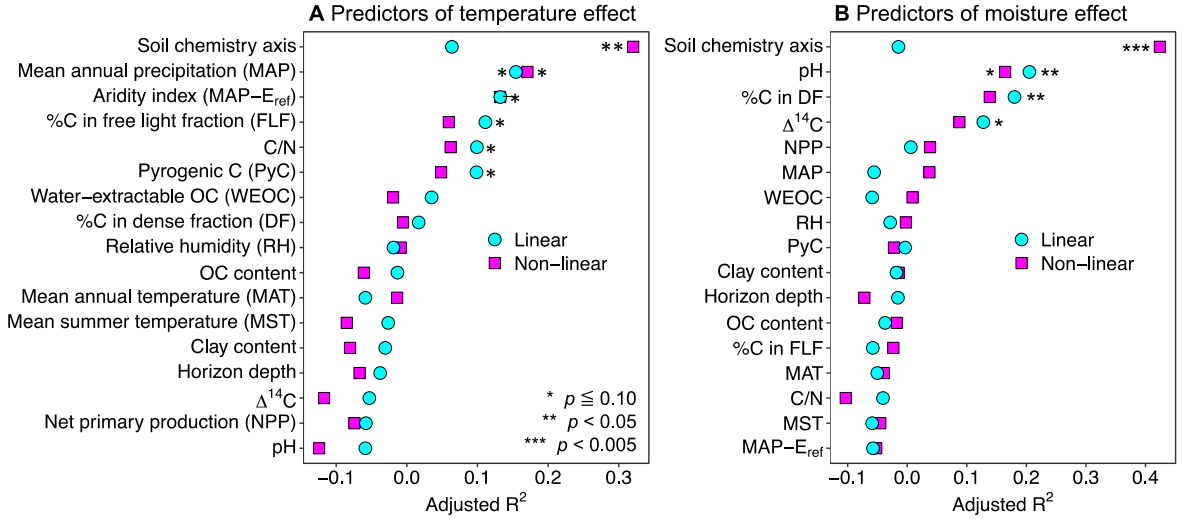

Figure 5. Ranking of soil and site properties as predictors of climate effects on CSR. Plots show adjusted R^2 from first-order (linear) and second-order (non-linear) polynomial regression for (A) temperature effects on CSR, or the difference between CSR at MST and MST +5 °C, and (B) moisture effects on CSR, or the difference between CSR at −33 and −400 kPa. E_{ref} = Hargreaves reference evaporation. Units for predictors are shown in Figure 4 caption. Additional fit parameters are listed in Tables S9 and S10.

chemistry subsystem, consistent with a shift in the dominant mechanism and degree of protection conferred by mineral SOC protection.

Soil Chemistry Effects on CSR Sensitivity to Temperature and Moisture. Increasing temperature and higher moisture generally increased CSR [i.e., ln(CSR ratio) > 0], but the response was not uniform across variation in soil chemistry (Figure 3). We detected a "U"-shaped, non-linear relationship between soil chemistry and temperature and moisture effects, where higher sensitivity to climate corresponded to higher abundance of either base cations or reactive metals (Figure 3A,B). The soil chemistry gradient was a significant predictor of both temperature and moisture effects using a second-order polynomial fit (Figures 3A,B and S6). Additionally, response to warming was greater than response to increased moisture in the reactive metal subsystem, whereas moisture effects were greater in the base cation subsystem (Figure 3C,D). The higher moisture sensitivity in base cation-dominated soils and temperature sensitivity with higher reactive metals did not depend on temperature or moisture treatment (i.e., no interactions were detected) (Figure 3C,D). Within the reactive metal subsystem, a slight trend toward higher temperature sensitivity at lower moisture levels (interaction p = 0.19) provides motivation for future finer-resolution experimental studies targeting temperature by moisture interactions in this subsystem.

The soil chemistry gradient also explained more variation in both temperature and moisture effects than a suite of site-level covariates, including RH, MAP, aridity, and NPP (Figures 4 and 5, S7, S8). The relationship between soil chemistry and sensitivity to temperature or moisture was also stronger than other soil properties and covariates often linked with SOC cycling, including soil pH, WEOC, clay content, total organic carbon (TOC), pyrogenic OC content, proportion of C in the

https://doi.org/10.1021/acs.est.1c04909
Environ. Sci. Technol. 2021, 55, 16224−16235

FLF and DF, and bulk C/N ratio (Figures 4 and 5, S9, S10). While the scarcity of detectable carbonates in this data set precluded use of the IC content as a continuous predictor variable, the effect of moisture was categorically higher (Wilcoxon Rank Sum p = 0.02) in the four sites with IC values > 0 wt % (0.37−2.25 wt %) (Figure S11). In contrast, the presence of carbonates did not affect response to temperature (Wilcoxon Rank Sum p = 0.41) (Figure S11).

Temperature Sensitivity. Due to the inherent temperature sensitivity of microbial processes involved in SOC destabilization, lower SOC bioavailability has been linked to higher SOC warming response.[31,66,67] Our observations are evidence that the type and reversibility of SOC-mineral stabilizing interactions should specifically be considered as a significant control on energy investment, and by extension, temperature sensitivity of SOC_{sub} mineralization. In soils with high non- or semi-crystalline Fe and Al and abundant reactive functional groups on mineral surfaces,[18] mineral-associated SOC (on average) is not expected to be as readily exchangeable with the soil solution under ambient conditions (i.e., without prolonged saturation).[26] Higher SOC-mineral bond stability may invoke temperature-sensitive microbial processes to overcome stabilizing interactions, such as production of extracellular chelating compounds.[26] The higher microbial energy investment to access reactive metal-stabilized SOC appears to provide a mechanistic explanation for previously observed relationships between temperature sensitivity and soil pH[67] or climate variables[68] correlated to reactive metal abundance (Figure 4). This relationship is also supported by higher temperature sensitivity of soil respiration in an Fe-rich soil relative to a 2:1 aluminosilicate-rich soil in a greenhouse experiment.[35]

Variation in temperature sensitivity as a function of SOC substrate quality[66−68] was also supported by weaker, but significant, linear relationships between temperature effects and proportion of SOC in the FLF, C/N ratio, and pyrogenic C content (Figure 5). Additionally, C/N ratio and pyrogenic C content were categorically higher in the reactive metal subsystem (Figure S3). Higher temperature effects on SOC mineralization were also correlated overall to decreased $CSR_{ambient}$ (Figure S12), indicating a link between sensitivity to warming and SOC bioavailability. The role of SOC substrate composition in mediating temperature response is also consistent with recent observations of enhanced aromatic and fatty acid C degradation in subsoils after in situ whole-profile warming.[69]

Together, these observations point toward subsoil temperature sensitivity as an interaction between SOC mineral protection and bioavailable SOC substrate composition that amplifies temperature sensitivity in higher reactive metal systems. In our study, the use of AO-extractable Fe and Al ties our observations of climate response to variation in non- or semi-crystalline Fe and Al phases. However, determination of differences among temperature responses as a function of mineralogical differences within relatively high reactive metal systems (e.g., differences in abundance of Fe vs Al-dominated minerals[70] or Fe and Al-to-Si ratios) may further clarify the specific role of organic substrate-reactive metal interaction reversibility.

Moisture Sensitivity. In contrast to reactive-metal associated SOC, electrostatic interactions facilitated by base cations are generally more easily reversible by changes in the soil solution (e.g., change in ionic strength or relatively small changes in pH), requiring less microbial energy investment.[24] Although soil solution chemistry is also affected by temperature, we propose that dependency on the presence of the soil solution for cation exchange processes contributed to the observed shift toward the higher effect of moisture on SOC mineralization in high base cation soils. Despite no significant difference in proportion of SOC in the DF between subsystems (Figure S3), greater DF SOC was significantly related to moisture effects only (Figure 5), consistent with a link between SOC substrate-mineral dynamics and sensitivity to moisture. In lower SOC, base cation-rich subsoils, spatial separation between microbes and SOC substrates may also drive higher dependence on the presence of the soil solution for microbe−substrate co-location.[29] In future studies, accounting for soil-specific differences in pore water dynamics would enable further assessment of the spatial dynamics of substrate−microbe−mineral interactions under changing moisture conditions.

Higher (but moisture-dependent) SOC bioavailability in the base cation subsystem is supported by overall higher ambient respiration (Figure 2). However, mean bulk SOC was categorically older (by proxy of the bulk radiocarbon content, $\Delta^{14}C$) (Figure S3), consistent with older bulk radiocarbon ages found in grassland NEON sites rich in base cations.[14] The larger range of $\Delta^{14}C$ in base cation-dominated systems and decoupling of $\Delta^{14}C$ and $CSR_{ambient}$ point toward greater diversity in mechanisms of mineral-driven SOC stabilization relative to reactive metal-dominated systems (e.g., a combination of electrostatic, inner-sphere, and/or inorganic−organic C interactions[14,22]). The inconsistent relationship between SOC bioavailability (i.e., decreased $CSR_{ambient}$) and moisture response (Figure S12) also illustrates that the SOC_{sub} stabilization mechanisms co-occurring in high base cation subsystems may not be equally sensitive to moisture. While the number of carbonate-rich soils in this study was small (n = 4), the higher median moisture response in carbonate-containing soils (Figure S11) provides motivation for further evaluation of carbonate effects on SOC_{sub} climate response.

Significance of Gradients in Soil Chemistry for Subsoil Carbon-Climate Feedbacks. The shift toward lower temperature but higher moisture effects in high base cation subsoils underscores the potential for systematic bias in Earth system models that apply scalar temperature or moisture corrections regardless of soil chemical properties (e.g., a fixed Q_{10} = 1.5 in the base version of CLM CN 5.0).[71] In this study, the Q_{10} of specific respiration deviated from 1.5 by approximately −50 to +100% (Figure S6). The soil chemistry gradient identified offers a tool to capture this variation, with potential for improved predictive capacity relative to commonly used proxies of mineral protection (e.g., clay content[72]) (Figure 5) and the additional benefit of a conceptual link to divergent mechanisms of SOC-mineral protection. In high base cation systems, potential underestimation of both temperature and moisture effects may substantially underestimate the predicted response of the mineral-stabilized component of SOC_{sub} to climate change. Though archetypical high reactive metal soils (e.g., Andisols) store a disproportionate amount of SOC, the higher base cation soil orders in this data set (e.g., Mollisols and Aridisols) together store approximately 30% of the global SOC stock.[73] Furthermore, higher base cation soils contained the oldest SOC in this study (Figure S3). Despite overall lower SOC concentrations, the total cumulative respiration flux (mg CO_2−C g $soil^{-1}$) was similar or higher overall compared to high reactive metal soils (Figure S13). Consequently, base cation-

https://doi.org/10.1021/acs.est.1c04909
Environ. Sci. Technol. 2021, 55, 16224−16235

dominated soil types may comprise a large, climate-sensitive SOC reservoir, regulated by complex SOC stabilization processes with accordingly complex climate sensitivities. Further experimental manipulations of divalent cation abundance may provide additional quantitative constraints on SOC climate response in these subsystems.

Enabled by controlled laboratory experiments, the factorial testing of temperature and moisture effects across a conterminous US soil property gradient in this study provides evidence that mineral surface interaction mechanisms at the nano- to microscale may propagate to ecosystem-scale SOC_{sub} response to climate change. As such, these insights support the need for future in situ studies of climate change effects on subsoil C flux that account for gradients in the dominant drivers of mineral SOC protection, in addition to ecological and physiological adaptations that may mitigate temperature or moisture response at longer timescales (e.g., shifts in vegetation, the soil microbiome, or soil chemical properties and mineralogy).[10,31,74,75] The potential for high warming response of soil respiration in tropical soils[33] also motivates the evaluation of system-dependent climate sensitivities, accounting for local soil chemical properties. Global subsoil measurements of both extractable base cations and reactive metals are imperative to the application of a framework for prediction of climate change response informed by the soil physicochemical gradient described here. Furthermore, climate response data spanning the gap between moderate and very high reactive metal-endmember sites (e.g., WREF in this data set), as well as additional carbonate-rich sites, would improve representation of variation in climate effects and prediction certainty.

This study targeted the effect of increasing moisture to field capacity on SOC mineralization, but projected climate change scenarios also include increased drought and precipitation event intensity,[76] both with potential implications for the release of mineral-protected SOC.[77,78] While approximately +5 °C warming in subsoils is possible under high-warming scenarios, the magnitude and rate of subsoil temperature changes are expected to vary across systems.[79] Future climate manipulation studies should therefore expand to include the multiple iterations of predicted variability in temperature and moisture regimes, including changes in the frequency of wet−dry cycles. Accounting for environmental controls on mineral-stabilized SOC could further reveal gaps in coupled climate-carbon model structures and enable more dynamic representation of SOC interactions and feedbacks.

DATA AVAILABILITY

The primary site, soil characterization, and incubation source data used in this study are available through the Environmental Data Initiative (https://doi.org/10.6073/pasta/99d113534ecaa04e820850e6169be04d).[80] All data are available on request to the authors.

ASSOCIATED CONTENT

Supporting Information

The Supporting Information is available free of charge at https://pubs.acs.org/doi/10.1021/acs.est.1c04909.

Methodological detail on site selection; radiocarbon and BPCA analyses; model RMSE estimation; data and information in support of site selection, experimental design, and incubation methodology; supporting soil characterization and incubation data; statistical results for polynomial regressions, correlations, and subsystem contrasts; and scatterplots and curve fits for polynomial regressions (PDF)

AUTHOR INFORMATION

Corresponding Author

Brian D. Strahm − *Department of Forest Resources and Environmental Conservation, Virginia Tech, Blacksburg, Virginia 24061, United States;* orcid.org/0000-0002-4025-2304; Phone: 540-231-8627; Email: brian.strahm@vt.edu; Fax: 540-231-3300

Authors

Angela R. Possinger − *Department of Forest Resources and Environmental Conservation, Virginia Tech, Blacksburg, Virginia 24061, United States;* Present Address: CUNY Advanced Science Research Center at the Graduate Center, City University of New York, New York, NY 10031, USA; Cary Institute of Ecosystem Studies, Millbrook, NY 12545, USA; orcid.org/0000-0003-2518-0979

Tyler L. Weiglein − *Department of Forest Resources and Environmental Conservation, Virginia Tech, Blacksburg, Virginia 24061, United States;* orcid.org/0000-0003-0656-7633

Maggie M. Bowman − *Environmental Studies Program, University of Colorado Boulder, Boulder, Colorado 80303, United States; Institute of Arctic and Alpine Research (INSTAAR), University of Colorado Boulder, Boulder, Colorado 80303, United States;* Present Address: Environmental and Molecular Sciences Laboratory, Pacific Northwest National Laboratory, Richland, WA 99354.

Adrian C. Gallo − *Department of Forest Engineering, Resources and Management, Oregon State University, Corvallis, Oregon 97331, United States*

Jeff A. Hatten − *Department of Forest Engineering, Resources and Management, Oregon State University, Corvallis, Oregon 97331, United States;* orcid.org/0000-0002-1685-6351

Katherine A. Heckman − *Northern Research Station, USDA Forest Service, Houghton, Michigan 49931, United States*

Lauren M. Matosziuk − *Department of Forest Engineering, Resources and Management, Oregon State University, Corvallis, Oregon 97331, United States;* orcid.org/0000-0001-9485-6886

Lucas E. Nave − *University of Michigan Biological Station, Pellston, Michigan 49769, United States; Department of Ecology and Evolutionary Biology, University of Michigan, Ann Arbor, Michigan 48109, United States*

Michael D. SanClements − *Institute of Arctic and Alpine Research (INSTAAR), University of Colorado Boulder, Boulder, Colorado 80303, United States; Battelle, National Ecological Observatory Network (NEON), Boulder, Colorado 80301, United States;* orcid.org/0000-0002-1962-3561

Christopher W. Swanston − *Northern Research Station, USDA Forest Service, Houghton, Michigan 49931, United States*

Complete contact information is available at: https://pubs.acs.org/10.1021/acs.est.1c04909

Notes

The authors declare no competing financial interest.

■ ACKNOWLEDGMENTS

Funding for this study was provided by the US National Science Foundation (awards EF-1340250, EF-1340681, and DBI-1724433). NEON is sponsored by the NSF and operated under cooperative agreement by Battelle. This material is based in part upon work supported by the NSF through the NEON program. We would like to thank Rommel Zulueta and the NEON SI Team for their support and assistance in the field for this project. Radiocarbon analysis was supported by the Radiocarbon Collaborative which is supported by the USDA Forest Service, University of California Irvine, and Michigan Technological University. Assistance with laboratory analyses was provided by Stephanie Duston and Dave Mitchem.

■ REFERENCES

(1) Batjes, N. H. Total carbon and nitrogen in the soils of the world. *Eur. J. Soil Sci.* **1996**, *47*, 151−163.

(2) Jobbágy, E. G.; Jackson, R. B. The vertical distribution of soil organic carbon and its relation to climate and vegetation. *Ecol. Appl.* **2000**, *10*, 423−436.

(3) Ciais, P.; Sabine, C.; Bala, G.; Bopp, L.; Brovkin, V.; Canadell, J.; Chhabra, A.; DeFries, R.; Galloway, J.; Heimann, M.; Jones, C.; Le Quéré, C.; Myneni, R. B.; Piao, S.; Thornton, P. Carbon and other biogeochemical cycles; *Climate Change 2013: The Physical Science Basis. Contribution of Working Group I to the Fifth Assessment Report of the Intergovernmental Panel on Climate Change*; Stocker, T. F., Qin, D., Plattner, G.-K., Tignor, M., Allen, S. K., Boschung, J., Nauels, A., Xia, Y., Bex, V., Midgley, P. M., Eds.; IPCC, Cambridge Univ. Press: Cambridge, U.K. and New York, NY, 2013; pp 465−570.

(4) Minasny, B.; Malone, B. P.; McBratney, A. B.; Angers, D. A.; Arrouays, D.; Chambers, A.; Chaplot, V.; Chen, Z.-S.; Cheng, K.; Das, B. S.; Field, D. J.; Gimona, A.; Hedley, C. B.; Hong, S. Y.; Mandal, B.; Marchant, B. P.; Martin, M.; McConkey, B. G.; Mulder, V. L.; O'Rourke, S.; Richer-de-Forges, A. C.; Odeh, I.; Padarian, J.; Paustian, K.; Pan, G.; Poggio, L.; Savin, I.; Stolbovoy, V.; Stockmann, U.; Sulaeman, Y.; Tsui, C.-C.; Vågen, T.-G.; van Wesemael, B.; Winowiecki, L. Soil carbon 4 per mille. *Geoderma* **2017**, *292*, 59−86.

(5) Wieder, W. R.; Harmann, M. D.; Sulman, B. N.; Wang, Y.-P.; Koven, C. D.; Bonan, G. B. Carbon cycle confidence and uncertainty: Exploring variation among soil biogeochemical models. *Glob. Change Biol.* **2018**, *24*, 1563−1579.

(6) Davidson, E. A.; Janssens, I. A. Temperature sensitivity of soil carbon decomposition and feedbacks to climate change. *Nature* **2006**, *440*, 165−173.

(7) Moyano, F. E.; Manzoni, S.; Chenu, C. Responses of soil heterotrophic respiration to moisture availability: An exploration of processes and models. *Soil Biol. Biochem.* **2013**, *59*, 72−85.

(8) Kleber, M.; Mikutta, R.; Torn, M. S.; Jahn, R. Poorly crystalline mineral phases protect organic matter in acid subsoil horizons. *Eur. J. Soil Sci.* **2005**, *56*, 717−725.

(9) Schmidt, M. W. I.; Torn, M. S.; Abiven, S.; Dittmar, T.; Guggenberger, G.; Janssens, I. A.; Kleber, M.; Kögel-Knabner, I.; Lehmann, J.; Manning, D. A. C.; Nannipieri, P.; Rasse, D. P.; Weiner, S.; Trumbore, S. E. Persistence of soil organic matter as an ecosystem property. *Nature* **2011**, *478*, 49−56.

(10) Hicks Pries, C. E.; Castanha, C.; Porras, R. C.; Torn, M. S. The whole-soil carbon flux in response to warming. *Science* **2017**, *355*, 1420−1423.

(11) Yan, D.; Li, J.; Pei, J.; Cui, J.; Nie, M.; Fang, C. The temperature sensitivity of soil organic carbon decomposition is greater in subsoil than in topsoil during laboratory incubation. *Sci. Rep.* **2017**, *7*, 5181.

(12) Salomé, C.; Nunan, N.; Pouteau, V.; Lerch, T. Z.; Chenu, C. Carbon dynamics in topsoil and subsoil may be controlled by different regulatory mechanisms. *Glob. Change Biol.* **2010**, *16*, 416−426.

(13) Chabbi, A.; Kögel-Knabner, I.; Rumpel, C. Stabilised carbon in subsoil horizons is located in spatially distinct parts of the soil profile. *Soil Biol. Biochem.* **2009**, *41*, 256−261.

(14) Heckman, K. A.; Nave, L. E.; Bowman, M.; Gallo, A.; Hatten, J. A.; Matosziuk, L. M.; Possinger, A. R.; SanClements, M.; Strahm, B. D.; Weiglein, T. L.; Rasmussen, C.; Swanston, C. W. Divergent controls on carbon concentration and persistence between forests and grasslands of the conterminous US. *Biogeochemistry* **2021**, *156*, 41−56.

(15) Nave, L. E.; Bowman, M.; Gallo, A.; Hatten, J. A.; Heckman, K. A.; Matosziuk, L.; Possinger, A. R.; SanClements, M.; Sanderman, J.; Strahm, B. D.; Weiglein, T. L.; Swanston, C. W. Patterns and predictors of soil organic carbon storage across a continental-scale network. *Biogeochemistry* **2021**, *156*, 75−96.

(16) Rasmussen, C.; Heckman, K.; Wieder, W. R.; Keiluweit, M.; Lawrence, C. R.; Berhe, A. A.; Blankinship, J. C.; Crow, S. E.; Druhan, J. L.; Hicks Pries, C. E.; Marin-Spiotta, E.; Plante, A. F.; Schädel, C.; Schimel, J. P.; Sierra, C. A.; Thompson, A.; Wagai, R. Beyond clay: towards an improved set of variables for predicting soil organic matter content. *Biogeochemistry* **2018**, *137*, 297−306.

(17) Deng, Y.; Dixon, J. B. Soil organic matter and organic-mineral interactions. In *Soil Mineralogy with Environmental Applications*; *SSSA Book Series No. 7*. Dixon, J. B., Shultze, D. G., Eds.; Soil Science Society of America: Madison, WI, 2002; pp 69−107.

(18) Kleber, M.; Eusterhues, K.; Keiluweit, M.; Mikutta, C.; Mikutta, R.; Nico, P. S. Mineral-organic associations: formation, properties, and relevance in soil environments. *Adv. Agron.* **2015**, *130*, 1−140.

(19) Lehmann, J.; Kleber, M. The contentious nature of soil organic matter. *Nature* **2015**, *528*, 60−68.

(20) Sarkar, B.; Singh, M.; Mandal, S.; Churchman, G. J.; Bolan, N. S. Chapter 3−Clay minerals-organic matter interactions in relation to carbon stabilization in soils. In *The Future of Soil Carbon−Its Conservation and Formation*; Garcia, C., Nannipieri, P., Hernandez, T., Eds.; Academic Press: Cambridge, MA, 2018; pp 71−86.

(21) Torn, M. S.; Trumbore, S. E.; Chadwick, O. A.; Vitousek, P. M.; Hendricks, D. M. Mineral control of soil organic carbon storage and turnover. *Nature* **1997**, *389*, 170−173.

(22) Rowley, M. C.; Grand, S.; Verrecchia, É. P. Calcium-mediated stabilization of soil organic carbon. *Biogeochemistry* **2018**, *137*, 27−49.

(23) Mouvenchery, Y. K.; Kučerík, J.; Diehl, D.; Schaumann, G. E. Cation-mediated cross-linking in natural organic matter: a review. *Rev. Environ. Sci. Biotechnol.* **2012**, *11*, 41−54.

(24) Von Lützow, M.; Kögel-Knabner, I.; Ekschmitt, K.; Matzner, E.; Guggenberger, G.; Marschner, B.; Flessa, H. Stabilization of organic matter in temperate soils: mechanisms and their relevance under different soil conditions − a review. *Eur. J. Soil Sci.* **2006**, *57*, 426−445.

(25) Mikutta, R.; Mikutta, C.; Kalbitz, K.; Scheel, T.; Kaiser, K.; Jahn, R. Biodegradation of forest floor organic matter bound to minerals via different binding mechanisms. *Geochim. Cosmochim. Acta* **2007**, *71*, 2569−2590.

(26) Bailey, V. L.; Pries, C. H.; Lajtha, K. What do we know about soil carbon destabilization? *Environ. Res. Lett.* **2019**, *14*, 083004.

(27) Kramer, M. G.; Chadwick, O. A. Climate-driven thresholds in reactive mineral retention of soil carbon at the global scale. *Nat. Clim. Change* **2018**, *8*, 1104−1108.

(28) Buettner, S. W.; Kramer, M. G.; Chadwick, O. A.; Thompson, A. Mobilization of colloidal carbon during iron reduction in basaltic soils. *Geoderma* **2014**, *221−222*, 139−145.

(29) Lehmann, J.; Hansel, C. M.; Kaiser, C.; Kleber, M.; Maher, K.; Manzoni, S.; Nunan, N.; Reichstein, M.; Schimel, J. P.; Torn, M. S.; Wieder, W. R.; Kögel-Knabner, I. Persistence of soil organic carbon caused by functional complexity. *Nat. Geosci.* **2020**, *13*, 529−534.

(30) Torn, M. S.; Swanston, C. W.; Castanha, C.; Trumbore, S. E. Storage and turnover of organic matter in soil. In *Biophysico-Chemical Processes Involving Natural Nonliving Organic Matter in Environmental*

https://doi.org/10.1021/acs.est.1c04909
Environ. Sci. Technol. 2021, 55, 16224−16235

Systems; Senesi, N., Xing, B., Huang, P. M., Eds.; John Wiley & Sons, Inc.: Hoboken, NJ, 2009; pp 219−272.
(31) Von Lützow, M.; Kögel-Knabner, I. Temperature sensitivity of soil organic matter decomposition − what do we know? *Biol. Fertil. Soils* **2009**, *46*, 1−15.
(32) Doetterl, S.; Berhe, A. A.; Arnold, C.; Bodé, S.; Fiener, P.; Finke, P.; Fuchslueger, L.; Griepentrog, M.; Harden, J. W.; Nadeu, E.; Schnecker, J.; Six, J.; Trumbore, S.; Van Oost, K.; Vogel, C.; Boeckx, P. Links among warming, carbon and microbial dynamics mediated by soil mineral weathering. *Nat. Geosci.* **2018**, *11*, 589−593.
(33) Nottingham, A. T.; Meir, P.; Velasquez, E.; Turner, B. L. Soil carbon loss by experimental warming in a tropical forest. *Nature* **2020**, *584*, 234−237.
(34) Chen, H.; Tian, H.-Q. Does a general temperature-dependent Q10 model of soil respiration exist at biome and global scale? *J. Integr. Plant Biol.* **2005**, *47*, 1288−1302.
(35) Thurgood, A.; Singh, B.; Jones, E.; Barbour, M. M. Temperature sensitivity of soil and root respiration in contrasting soils. *Plant Soil* **2014**, *382*, 253−267.
(36) Wang, T.; Hamann, A.; Spittlehouse, D. L.; Murdock, T. Q. ClimateWNA—High-resolution spatial climate data for western North America. *J. Appl. Meteorol. Climatol.* **2012**, *51*, 16−29.
(37) ORNL DAAC. *MODIS and VIIRS Land Products Fixed Sites Subsetting and Visualization Tool*; ORNL DAAC: Oak Ridge, TN, 2018. https://doi.org/https://doi.org/10.3334/ORNLDAAC/1567 (accessed Jan 31, 2020); Subset obtained for MOD17A3H product at various sites in Spatial Range: N = 47.16 N, S = 28.13 N, E = 76.56 W, W = 122.33 W, time period: 2005-01-01 to 2014-01-01, and subset size: 0.5 × 0.5 km.
(38) Running, S.; Mu, Q.; Zhao, M. *MOD17A3H MODIS/Terra Net Primary Production Yearly L4 Global 500m SIN Grid V006*; NASA EOSDIS Land Processes DAAC, 2018.
(39) PRISM Climate Group, Oregon State University. Prism Climate Data; Mean temp, 30-year normal; 1981-2010 (monthly and annual), 800 m resolution; PRISM Climate Group, Oregon State University: Corvallis, OR. http://prism.oregonstate.edu (accessed July 15, 2016).
(40) Soil Survey Staff. Soil Survey Field and Laboratory Methods Manual. In *Soil Survey Investigations Report No. 51, Version 2.0*; Burt, R., Ed.; U.S. Department of Agriculture, Natural Resources Conservation Service, 2014.
(41) Shang, C.; Zelazny, L. W. Selective dissolution techniques for mineral analysis of soils and sediments. In *Methods of Soil Analysis Part 5−Mineralogical Methods, 5.5*; Ulery, A. L., Drees, L. R., Eds.; Soil Science Society of America, Inc.: Madison, WI, 2008; pp 33−80.
(42) Inagaki, T. M.; Possinger, A. R.; Grant, K. E.; Schweizer, S. A.; Mueller, C. W.; Derry, L. A.; Lehmann, J.; Kögel-Knabner, I. Subsoil organo-mineral associations under contrasting climate conditions. *Geochim. Cosmochim. Acta* **2020**, *270*, 244−263.
(43) Possinger, A. R.; Bailey, S. W.; Inagaki, T. M.; Kögel-Knabner, I.; Dynes, J. J.; Arthur, Z. A.; Lehmann, J. Organo-mineral interactions and soil carbon mineralizability with variable saturation cycle frequency. *Geoderma* **2020**, *375*, 114483.
(44) Fisher, P.; Aumann, C.; Chia, K.; O'Halloran, N.; Chandra, S. Adequacy of laser diffraction for soil particle size analysis. *PLoS One* **2017**, *12*, No. e0176510.
(45) Yang, Y.; Wang, L.; Wendroth, O.; Liu, B.; Cheng, C.; Huang, T.; Shi, Y. Is the laser diffraction method reliable for soil particle size distribution analysis? *Soil Sci. Soc. Am. J.* **2019**, *83*, 276−287.
(46) Thomas, G. W. Soil pH and soil acidity. In *Methods of Soil Analysis, Part 3 Chemical Methods*; Sparks, D. L., Page, A. L., Helmke, P. A., Loeppert, R. H., Soltanpour, P. N., Tabatabai, M. A., Johnston, C. T., Sumner, M. E., Eds.; Soil Science Society of America and America Society of Agronomy: Madison, WI, 1996; pp 475−490.
(47) Harris, D.; Horwáth, W. R.; van Kessel, C. Acid fumigation of soils to remove carbonates prior to total organic carbon or CARBON-13 isotopic analysis. *Soil Sci. Soc. Am. J.* **2001**, *65*, 1853−1856.
(48) Vogel, J. S.; Southon, J. R.; Nelson, D. E. Catalyst and binder effects in the use of filamentous graphite for AMS. *Nucl. Instrum. Methods Phys. Res., Sect. B* **1987**, *29*, 50−56.
(49) Davis, J. C.; Proctor, I. D.; Southon, J. R.; Caffee, M. W.; Heikkinen, D. W.; Roberts, M. L.; Moore, T. L.; Turteltaub, K. W.; Nelson, D. E.; Loyd, D. H.; Vogel, J. S. LLNL/US AMS facility and research program. *Nucl. Instrum. Methods Phys. Res., Sect. B* **1990**, *52*, 269−272.
(50) Stuiver, M.; Polach, H. A. Discussion: reporting of ^{14}C data. *Radiocarbon* **1977**, *19*, 355−363.
(51) Matosziuk, L. M.; Alleau, Y.; Kerns, B. K.; Bailey, J.; Johnson, M. G.; Hatten, J. A. Effects of season and interval of prescribed burns on pyrogenic carbon in ponderosa pine stands in the southern Blue Mountains, Oregon, USA. *Geoderma* **2019**, *348*, 1−11.
(52) Golchin, A.; Oades, J.; Skjemstad, J.; Clarke, P. Soil structure and carbon cycling. *Aust. J. Soil Res.* **1994**, *32*, 1043−1068.
(53) Golchin, A.; Oades, J.; Skjemstad, J.; Clarke, P. Study of free and occluded particulate organic matter in soils by solid state ^{13}C Cp/MAS NMR spectroscopy and scanning electron microscopy. *Aust. J. Soil Res.* **1994**, *32*, 285−309.
(54) Strickland, T. C.; Sollins, P. Improved method for separating light- and heavy-fraction organic material from soil. *Soil Sci. Soc. Am. J.* **1987**, *51*, 1390−1393.
(55) Swanston, C. W.; Torn, M. S.; Hanson, P. J.; Southon, J. R.; Garten, C. T.; Hanlon, E. M.; Ganio, L. Initial characterization of processes of soil carbon stabilization using forest stand-level radiocarbon enrichment. *Geoderma* **2005**, *128*, 52−62.
(56) Weiglein, T. L.; Strahm, B. D.; Bowman, M. M.; Gallo, A. C.; Hatten, J. A.; Heckman, K. A.; Matosziuk, L. M.; Nave, L. E.; Possinger, A. R.; SanClements, M. D.; Swanston, C. W. Key predictors of soil organic matter vulnerability to mineralization differ with depth at a continental scale. *Biogeochemistry* **2021**, DOI: 10.1007/s10533-021-00856-https://doi.org/10.1007/s10533-021-00856-x.
(57) R Core Team. *R: A Language and Environment for Statistical Computing*; R Foundation for Statistical Computing: Vienna, Austria, 2019. https://www.R-project.org/.
(58) RStudio Team. *RStudio: Integrated Development for R*; RStudio, Inc.: Boston, MA, 2017. http://www.rstudio.com/.
(59) Lloyd, J.; Taylor, J. A. On the temperature dependence of soil respiration. *Funct. Ecol.* **1994**, *8*, 315−323.
(60) Saxton, K. E.; Rawls, W. J.; Romberger, J. S.; Papendick, R. I. Estimating generalized soil-water characteristics from texture. *Soil Sci. Soc. Am. J.* **1986**, *50*, 1031−1036.
(61) Harris, R. F.; Parr, J. F. Effect of water potential on microbial growth and activity. In *Water Potential Relations in Soil Microbiology*; Gardner, W. R., Elliot, L. F., Eds.; Soil Science Society of America, Inc.: Madison, WI, 1981; Vol. 9, pp 23−95.
(62) NEON (National Ecological Observatory Network). Soil Physical Properties, Megapit (DP1.00096.001). http://data.neonscience.org (accessed Jan 10, 2018).
(63) Soil Survey Staff, USDA, NRCS. Web Soil Survey. https://websoilsurvey.sc.egov.usda.gov/App/HomePage.htm (accessed Jan 10, 2018).
(64) Tamir, G.; Shenker, M.; Heller, H.; Bloom, P. R.; Fine, P.; Bar-Tal, A. Can soil carbonate dissolution lead to overestimation of soil respiration? *Soil Sci. Soc. Am. J.* **2011**, *75*, 1414−1422.
(65) Fox, J.; Weisberg, S. *An {R} Companion to Applied Regression*, 3rd ed.; Sage: Thousand Oaks, CA, 2019. https://socialsciences.mcmaster.ca/jfox/Books/Companion/.
(66) Hartley, I. P.; Ineson, P. Substrate quality and the temperature sensitivity of soil organic matter decomposition. *Soil Biol. Biochem.* **2008**, *40*, 1567−1574.
(67) Craine, J.; Spurr, R.; McLauchlan, K.; Fierer, N. Landscape-level variation in temperature sensitivity of soil organic carbon decomposition. *Soil Biol. Biochem.* **2010**, *42*, 373−375.
(68) Zhou, T.; Shi, P.; Hui, D.; Luo, Y. Global pattern of temperature sensitivity of soil heterotrophic respiration (Q_{10}) and its

implication for carbon-climate feedback. *J. Geophys. Res.* **2009**, *114*, G02016.
(69) Ofiti, N. O. E.; Zosso, C. U.; Soong, J. L.; Solly, E. F.; Torn, M. S.; Wiesenberg, G. L. B.; Schmidt, M. W. I. Warming promotes loss of subsoil organic carbon through accelerated decomposition of plant-derived organic matter. *Soil Biol. Biochem.* **2021**, *156*, 108185.
(70) Kirsten, M.; Mikutta, R.; Vogel, C.; Thompson, A.; Mueller, C. W.; Kimaro, D. N.; Bergsma, H. L. T.; Feger, K.-H.; Kalbitz, K. Iron oxides and aluminous clays selectively control soil carbon storage and stability in the humid tropics. *Sci. Rep.* **2021**, *11*, 5076.
(71) Lawrence, D.; Andrew, B.; Bonan, G.; Ghimire, B.; van Kampenhout, L.; Kennedy, D.; Kluzek, E.; Knox, R.; Lawrence, P.; Li, F.; Li, H.; Lombardozzi, D.; Lu, Y.; Perket, J.; Riley, W.; Sacks, W.; Shi, M.; Wieder, W.; Xu, C. *Technical Description of Version 5.0 of the Community Land Model (CLM)*; National Center for Atmospheric Research, University Corporation for Atmospheric Research: Boulder, CO, 2018.
(72) Wieder, W. R.; Grandy, A. S.; Kallenbach, C. M.; Bonan, G. B. Integrating microbial physiology and physio-chemical principles in soils with the Microbial-Mineral Carbon Stabilization (MIMICS) model. *Biogeosciences* **2014**, *11*, 3899−3917.
(73) Eswaran, H.; Reich, P. F.; Kimble, J. M.; Beinroth, F. H.; Padmanabhan, E.; Moncharoen, P. Global carbon stocks. In *Global Climate Change and Pedogenic Carbonates*; Lal, R., Kimble, J. M., Stewart, B. A., Eswaran, H., Eds.; Lewis: Boca Raton, FL, 1999.
(74) Subke, J.-A.; Bahn, M. On the "temperature sensitivity" of soil respiration: Can we use the immeasurable to predict the unknown? *Soil Biol. Biochem.* **2010**, *42*, 1653−1656.
(75) Zosso, C. U.; Ofiti, N. O. E.; Soong, J. L.; Solly, E. F.; Torn, M. S.; Huguet, A.; Wiesenberg, G. L. B.; Schmidt, M. W. I. Whole-soil warming decreases abundance and modifies the community structure of microorganisms in the subsoil but not in surface soil. *Soil* **2021**, *7*, 477−494.
(76) Christensen, J. H.; Krishna Kumar, K.; Aldrian, E.; An, S.-I.; Cavalcanti, I. F. A.; de Castro, M.; Dong, W.; Goswami, P.; Hall, A.; Kanyanga, J. K.; Kitoh, A.; Kossin, J.; Lau, N.-C.; Renwick, J.; Stephenson, D. B.; Xie, S.-P.; Zhou, T. Climate phenomena and their relevance for future regional climate change. *Climate Change 2013: The Physical Science Basis. Contribution of Working Group I to the Fifth Assessment Report of the Intergovernmental Panel on Climate Change*; Stocker, T. F., Qin, D., Plattner, G.-K., Tignor, M., Allen, S. K., Boschung, J., Nauels, A., Xia, Y., Bex, V.; Midgley, P. M., Eds.; Cambridge University Press: Cambridge, U.K., 2013; pp 1217−1308.
(77) Huang, W.; Hall, S. J. Elevated moisture stimulates carbon loss from mineral soils by releasing protected organic matter. *Nat. Commun.* **2017**, *8*, 1774.
(78) Cleveland, C. C.; Wieder, W. R.; Reed, S. C.; Townsend, A. R. Experimental drought in a tropical rain forest increases soil carbon dioxide losses to the atmosphere. *Ecology* **2010**, *91*, 2313−2323.
(79) Soong, J. L.; Phillips, C. L.; Ledna, C.; Koven, C. D.; Torn, M. S. CMIP5 models predict rapid and deep soil warming over the 21st century. *J. Geophys. Res.: Biogeosci.* **2020**, *125*, No. e2019JG005266.
(80) Nave, L. E.; Heckman, K. A.; Bowman, M.; Gallo, A. C.; Hatten, J.; Matosziuk, L.; Possinger, A. R.; SanClements, M.; Strahm, B. D.; Weiglein, T. L.; Swanston, C. Soil Organic Matter Mechanisms of Stabilization (SOMMOS) - enhanced soil characterization data from 40 National Ecological Observatory Network (NEON) sites ver 2. *Environmental Data Initiative*, 2021, DOI: 10.6073/pasta/99d113534ecaa04e820850e6169be04d.

https://doi.org/10.1021/acs.est.1c04909
Environ. Sci. Technol. 2021, 55, 16224−16235